Determination of the Boltzmann Constant through Various Methods in Optical Trapping

Vedang Lad, Bryan Sperry*
MIT Department of Physics
(Dated: January 27, 2022)

Optical trapping is one of the most powerful methods in biophysics today. Using an infrared laser, optical traps interact with micron sized dielectric objects by applying and measuring forces on the piconewton scale. We measure the Brownian motion and Stokes drag of a 3.71 μm bead. Analysis performed using the Power Spectrum Decomposition(PSD) resulted in Boltzmann constant of $1.755 \pm 0.577 \times 10^{-23}$ while the Stokes drag experiment and the Equipartition Theorem resulted in a Boltzmann constant of $2.54 \pm 4.60 \times 10^{-24}$.

I. INTRODUCTION

Since its discovery in 1970 by Arthur Ashkin, [1] optical trapping has become an influential part of biophysics. It relies on the fact that light has momentum and therefore imparts a force. This force, when refracted on dielectric objects, can allow you to trap and therefore move the objects with the infrared laser. For this experiment, we work with 3.71 μm micro-spheres that are placed in a thin layer of water and under the microscope of the optical trap. To generate meaningful data, we carry out two forms of calibration, position calibration, and stiffness calibration. These calibrations are crucial to get the best data from the optical trap. Finding more accurate calibration methods is an important field of research in optical trapping [3].

Following the calibration, we determine the trap stiffness and the Boltzmann constant using two independent methods of data collection and analysis. The first method is obtaining both α and k_B using Brownian Motion and PSD. The second method is to determine α through Stokes drag and then solve for k_B using the equipartition theorem. It is important to note that measurement and eventual analysis done in the x direction is independent of that of y direction so each method generates two values of k_b.

Most modern techniques to determine the Boltzmann constant utilize thermometry. These experiments measure interactions of gases in vacuums while varying electric fields and varying frequencies of sounds. Most recent measurements of the k_B boast uncertainty values in one in 5 million [2].

II. THEORETICAL REMARKS

II.1. Physics of Optical Trapping

The purpose of the laser is to place the dielectric object in a position of stable equilibrium. This is achieved through the presence of two forces, the *scattering force* and the *gradient force*[4]. The scattering force points in the direction of the laser and the gradient force against the direction of the beam. When the laser passes through the center, these forces balance and the micro-sphere is "trapped". As seen in FIG 1, as the bead deviates from the center, the scattering force and the gradient force point in the opposing direction.[4]This restoring force is analogous to the "spring" constant k which we will refer to as α.

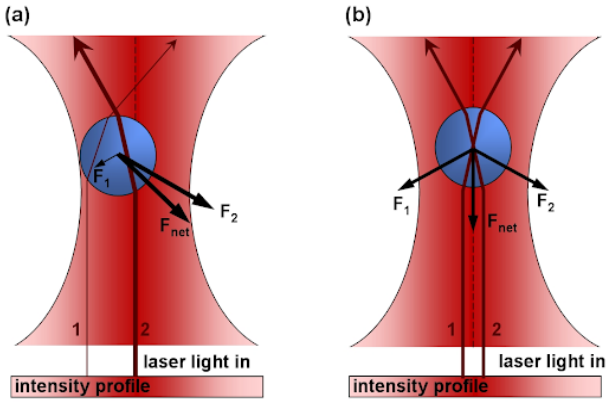

FIG. 1. The laser travels from bottom to top. When the laser beam is focused through the center in the right, the two forces balance each other out and the bead is stabilized. Note that the intensity profile can be seen in the red gradient. This generates the gradient force that opposes the direction of the scattering force. In the figure this is F_1 and F_2

II.2. Method 1: Brownian Motion and the Power Spectral Distribution (PSD) Function

Brownian Motion is the random uncontrolled movement of particles due to collisions with other molecules [4]. Measurement of this motion reveals random displacement which can also be characterized by a spectrum [4]. If each impact is random, then the forces on the particle may only be correlated for only a short time. Approximating this to zero, reveals a spectrum of "*white noise*" [4]. Based on the size of the trapped bead, we assume an

* vedlad@mit.edu; http://web.mit.edu/8.13/

over-damped oscillation regime [5] which results in the equation of motion:

$$\beta\dot{x} + \alpha x = F(t), \tag{1}$$

Where we have that β is hydrodynamic drag coefficient, α is the harmonic optical trap of stiffness, d is the diameter of the bead, η is the viscosity of the medium. We also define β as

$$\beta = 3\pi\eta d, \tag{2}$$

Using the viscosity of water $\eta = 8.90 \times 10^{-4}$ Pa*s and the fact that we use $3.71\mu m$ beads, we find that $\beta = 3.111 \times 10^{-8}$ Pa*s

In order see this spectrum, we must Fourier Transform the equation of motion. Utilizing the Wiener-Khinchin theorem we have the PSD

$$S_{xx} = \frac{k_b T}{\pi^2 \beta (f^2 + {f_0}^2)} \tag{3}$$

where $f_0 = \frac{\alpha}{2\pi\beta}$

II.3. Method 2: Equipartition Theorem and Stokes-Drag

In statistical physics, the Boltzmann constants represents the relationship between kinetic energy and temperature. Viewing temperature as the fluctuations of force imparted on the gas, allows us to utilize the equipartition theorem. This theorem assigns each degree of freedom to have $\frac{1}{2}k_B T$ energy. Therefore a single particle trapped in a harmonic potential would have energy $\frac{1}{2}\alpha\langle x^2\rangle$, where α is the same trap stiffness. The variance $\langle x^2\rangle$ arises naturally out of the measured Brownian motion, where x is the displacement from the center of a trapped beam. Equating the two energies, we come to the equation

$$\frac{1}{2}k_b T = \frac{1}{2}\alpha\langle x^2\rangle \tag{4}$$

To obtain α, we measure the Stokes Drag experienced by optically trapped particles. This is when the movement of a fluid around a particle is large enough that the Brownian motion can be ignored. The equation of motion simplifies to

$$\alpha x = \beta\nu \tag{5}$$

where ν is the stage velocity. Using this method, we can obtain α, which we can then put into equation (4). With the variance from the Brownian motion and α from the Stokes Drag, we can finally solve for the Boltzmann constant.

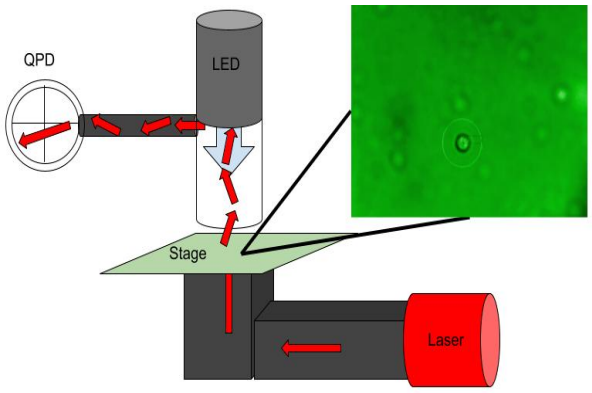

FIG. 2. A simplified setup of the optical trap. A laser enters from the bottom of the stage and interacts with the particles and fluid in the stage. It is then refracted due to its interactions (or not) and lands on the QPD. The LED allows for the microscope to see a live feed through a computer, as seen by the image with a bead focused on the screen

III. EXPERIMENTAL ARRANGEMENT

III.1. Apparatus

The optical trap consists of three essential parts. The Quadrant Photodetector (QPD), a motorized stage, and a laser as what is seen in FIG.2. Variations in the laser and the stage movement are what allow us to obtain various values of k_B. Note that the LED, which is essential to find a bead, does not contribute to any of the particle light interactions that occur. It is only utilized by the camera. The QPD consists of a photo-diode that measures the position of the scattered laser light in millivolts. More specifically, The QPD responds to position changes less than 100 μs [4] which is essential to measure the response of the bead. The motorized stage is controlled by a network of Piezo actuators which are driven by high voltage strain gauges. The position here is measured in volts, which represents the voltage across the strain gauge. Converting the QPD and Piezo from voltage to position in μm is the first part of the calibration.

III.2. Calibration and Data Collection

The position calibration is conducted on beads placed in a NaCl solution. This solution allows for the beads to sink and then "*stick*" to the bottom of the coverslip. Stuck beads are then "*scanned*" over the center in the X and Y directions at 5 laser levels, from 100 mA laser to 200 mA at intervals of 25 mA. At every laser power, the bead is scanned 10 times in the X and Y direction each. Note that these intervals correspond exactly to the intervals that are used in the Brownian motion measurements and the Stokes Drag measurements. Using these scans we

FIG. 3. A photograph of the Piezo controllers that control the stage. Data points of position taken at different voltages allow for the extraction of the linear relationship, essential for position calibration.

extract a linear relationship between the QPD X(Y) and Piezo X (Y). The final portion of the calibration requires extracting the conversion between Piezo X (Y) and Position X (Y). This conversion factor is extracted by taking arbitrary data points by deviating the stage position and noting the change in voltage. The relationship is once again extracted through the slope of the points.

Stiffness Calibration for Method 1 is extracted from the PSD and discussed in subsequent sections. For method 2, stiffness calibration is extracted through the Stokes Drag experiment. In this portion of the experiment, the bead is free to move in water, not NaCl. The Piezos oscillation amplitude and frequency are controlled externally through a computer so that there is no Brownian motion. It is important to not oscillate the stage too fast that the bead begins to move outside of the linear regime which is no longer characterized by Stokes drag. Once again, we collect data at the same laser levels that we have position calibrated for. The data collection for Brownian motion is identical to that of the Stokes Drag, however, we turn off stage oscillations and just measure the random movement of a trapped bead.

IV. DATA AND ANALYSIS

IV.1. Calibration

Scanning over the center of the bead results in a QPD scan that looks like the one presented in FIG 4. Data across all laser levels results in the linear relationship that is seen in FIG 5. Since the data in Figure 4 is only linear in a particular region about the center, it was important to conduct 10 trials and obtain an average value. This average value with the corresponding error is seen in FIG 5. To fit the data best, the data were binned in x and y, then subsequently fit based on the error that was generated from the bin. The error in a given bin is characterized by one standard deviation from the mean. The second portion of the calibration data, between the stage and the position, is seen in FIG 6. This portion of the calibration only depends on the position of the Piezo and not on a bead. Errors here come from the uncertainty seen by the Piezo values. With repeated trials, all of the calibration data resulted in small uncertainties in the X and Y direction. The fit for both of these plots resulted in a 99% Chi-Squared probability, which was expected. Both of these complete the position calibration needed for both methods in the experiment. Note that all of the plots presented are for QPD X and/or Piezo X and at 100mA for consistency.

IV.2. Brownian Motion and the Power Spectral Distribution (PSD) Function

For the Brownian Motion, we can see in FIG 9 that the motion of the bead is random and completely uncorrelated. To fit equation 3, we first took the QPD data and Fourier transformed it. This was done using the Welch method [6], which provides a Fast Fourier Transform method to estimate the power spectrum. For the PSD method of analysis, the Fourier Transformation resulted in a dense, oscillatory plot as seen in FIG 12. Fits on this spectrum repeatedly failed due to a large number of terms on the Fourier series producing noise. In place of truncating values on the Fourier series, we chose a method that would still utilize all the data available. To extract a higher quality power spectrum we binned each point separately, by taking the average of the neighboring points. The mean value of the bin takes on the new value of the PSD at that frequency, and the standard deviation is the new error. The new spectrum, as seen as the black-colored spectrum in FIG 12, is then fitted using 3. Doing this for all laser levels, we obtain the plot seen in FIG 8. All lines in FIG 8, which were fitted independently, clearly taper off at a set frequency. Also notice that the order of the lines corresponds to the current of the laser. This spectrum likely has to be filtered at early energies but was not done so because the spectral range of the QPD was unknown. Without knowing its threshold, truncation may remove data essential to the fit. Using these fits, we can extract the values of α which can be seen in FIG 10. While QPD X and QPD Y both increase in stiffness as current increase, FIG 10 clearly shows a greater increase in Y than X. There is a clear break in symmetry here in X and Y and likely due to errors, discussed later. All in all, from method 1, we find that $k_b = 1.755 \pm 0.577 \times 10^{-23} J/K$.

IV.3. Equipartition Theorem and Stokes-Drag

The variance of the Brownian motion data allows us to obtain $\langle x^2 \rangle$ in equation 4. The data from the Stokes drag experiment resulted in an extremely non-linear relationship. It was evident that at the tail ends of the oscillation, the bead exited the linear region of the oscillation and no longer could be characterized by Stokes Drag. To extract the linear region from the data, the ends of the data were clipped evenly about the center. After narrowing the range of oscillation between 0.4 around the

center point, we see in the linear relationship in FIG 7. The value of 0.4 came from starting at the ends of the plot and moving inwards from the ends while attempting to fit a line. The fit was binned, both in the x and y direction, as done previously. The best chi2 fit resulted from the plot that is seen in FIG 7. This line is represented by equation 5, where we now have a value for α. Likely due to the unknown artifacts in the plot, we can see in FIG 11 that the trap stiffness is different from the one seen in FIG 10. While trap stiffness should increase for higher laser power, this is not the case for X. Taking our value of α and plugging it into equation 4 we can finally solve for the values of the Boltzmann constant. From method 2, we find that $k_b = 2.54 \pm 4.60 \times 10^{-24} J/K$

IV.4. Uncertainties

Working on micron scales and a large dependence on electronics results in an extremely difficult characterization of the error. During analysis, this was combated with filtering data where possible using the binning technique described above. One of the largest sources of error likely comes from the laser. As seen by equation 3 and equation 4, the temperature is an important part of determining the Boltzmann constant. While we tried to constantly move the bead to reduce the heating of the water, this likely still resulted in a large unquantifiable error. Therefore our temperature uncertainty of about 5 K, is likely higher. As seen on many of the plots, we see growing uncertainties as the current in the laser increases which propagates throughout the experiment. We assign an uncertainty of 5% to the Piezo electronics, as errors in Piezo electronics are extremely difficult to detect since they move smaller than the micron scale. Small inconsistencies in the Piezo movement can result in drastic changes in the data. The 5 percent value is extracted from the calibration data in FIG 4, where across 10 trials, the largest deviation at a given point was upper bounded by 5%. We assign a 3% error to the difference in the index of refraction of the calibration data, which used a salt solution for the fixed bead, as opposed to water utilized in the remaining experiment. We assign a 1% error to all other errors which may have gone unaccounted for.

Heating due to laser	10%
Piezo electronics (strain gauge)	5%
Lens and coverslip	3%
Other	1%

V. SUMMARY

We have presented two different methods of obtaining data and analyzing them independently. Method 1,

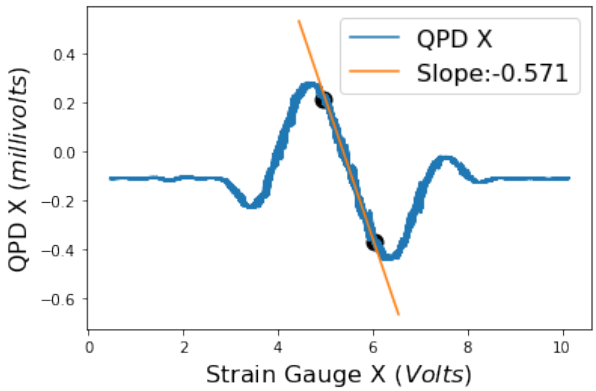

FIG. 4. An example of an X Scan over a fixed bead. This was one of 10 trials over the center of the bead taken at 100 mA on the laser. The fitted slope in yellow represents the relationship between the QPD and Piezo which is essential for the position calibration.

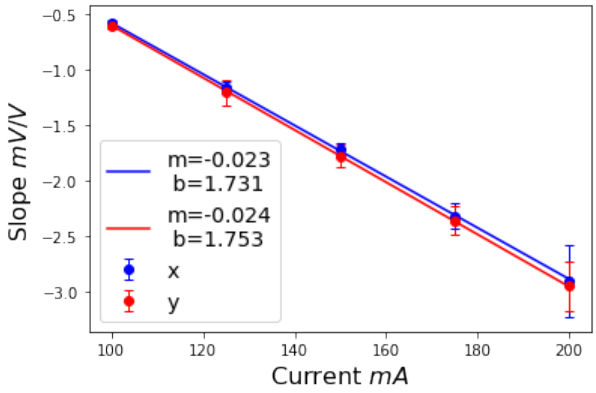

FIG. 5. The fitted line shows how the slope, QPD/Piezo, changes as we increase the current in the laser. While X and Y are separated here, they are within error of one another. This are the same values and uncertainties that will be propagated to the remainder experiment which allow the conversion to position in μ, in conjunction with FIG 6

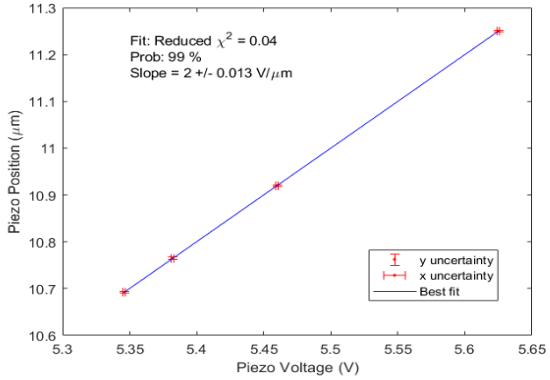

FIG. 6. The two fitted line shows how the slope, Piezo/Position, changes as we increase the current in the laser. This in conjunction with FIG 5 complete the position calibration

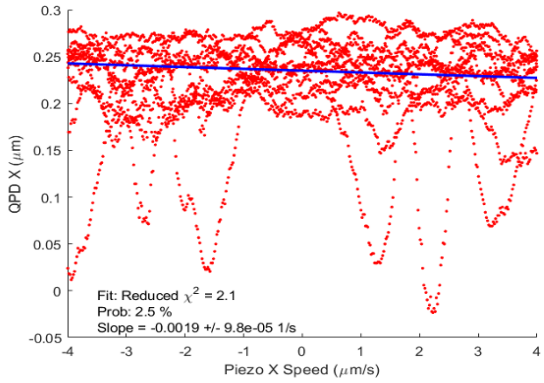

FIG. 7. This represents the Stokes drag at 100 mA after the range of the oscillation of the original stokes data was limited between -0.4 and 0.4. The blue fitted line is a fit that was done from the data after it was binned in both the x-direction and the y-direction. Artifacts seen below the line of fit are unknown but may arise due to the motion of the stage

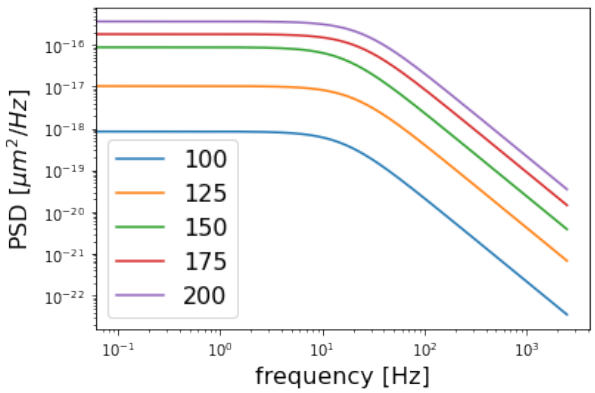

FIG. 8. This represents all of the fits of the PSD of various laser currents. Notice that regardless of the power, all of the fits taper off at the same point. Since all fits were independent of one another, this characterizes an important relationship seen in equation 3.

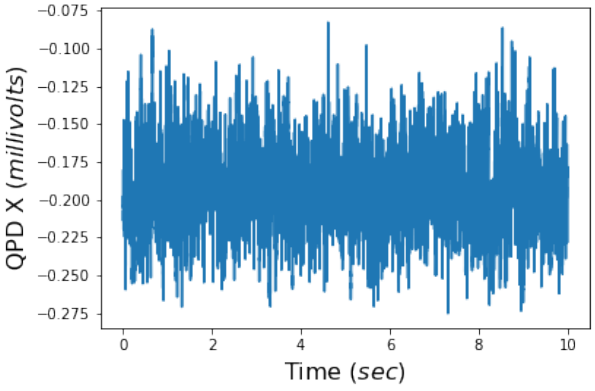

FIG. 9. The position of the bead in the plot above characterizes a random relationship about the center of its axis with no noticeable trend.

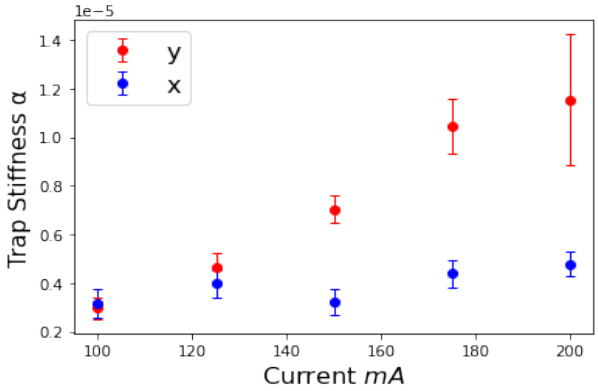

FIG. 10. Here we obtain the stiffness calibration that results from the PSD. After each PSD is fit at different laser currents, it exhibits a growing relationship. As the laser power increases, the stiffness of the trap also increases as the bead is more trapped.

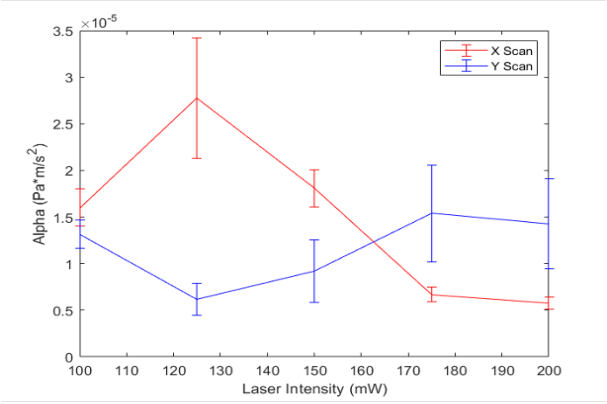

FIG. 11. The stiffness calibration of the stokes drag data does not reveal the same relationship as the PSD method did. While there is an initial increase X, it is followed by an overall decrease. On the other hand, there is an initial and final decrease in Y scan but an over increase throughout. All in all, suggest the X scan may be dominated by uncertainties

which extracts both trap stiffness and the Boltzmann constant using the PSD. Method 2 relies on Stokes Drag and the Equipartition Theorem. A difference in a factor of 10 suggests large domination of uncertainties in the method behind both experiments. These effects likely grew larger uncertainties in method 2 which relied on two measurements to determine the Boltzmann constant instead of method 1, which had multiple trials and a single fit. With method 1 we obtained $k_b = 1.755 \pm 0.577(stat) \pm 0.333(sys) \times 10^{-23} J/K$, while method 2 we obtained $k_b = 2.54 \pm 4.60(stat) \pm 0.48(sys) \times 10^{-24} J/K$. Method 1, with fewer effects of uncertainties, was within range of the theoretical value of the Boltzmann constant [2], which is $1.380649 \times 10^{-23} J/K$. Where Method 2 suggests data largely dominated with uncertainties in measurement.

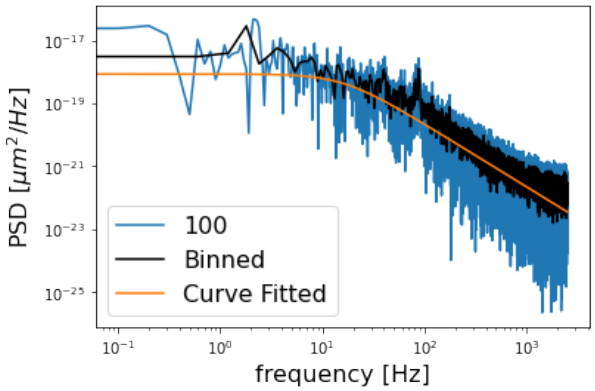

FIG. 12. This diagram depicts the three steps that were taken to extract the line of best fit. First, the QPD value is Fourier transformed. Then the Fourier transform is binned where each bin has a mean value and standard deviation, which we treat as an error. The binned spectrum is characterized by the black line. This mean value takes on the new value of a given frequency which is then fit by the orange line. The line presents a CHI2 probability of 0.64

ACKNOWLEDGMENTS

We gratefully acknowledge the help of Sean Robinson, Professor Paus for generously granting an extension, Welch for his numerical method, and Arthur Ashkin for his genius in discovering optical trapping.

[1] A. Ashkin, "Acceleration and trapping of particles by radiation pres- sure," Phys. Rev. Lett. 24(4), 156 (1970).

[2] Benz, S. , Pollarolo, A. , Qu, J. , Rogalla, H. , Urano, C. , Tew, W. , Dresselhaus, P. and White, D. (2011), An electronic measurement of the Boltzmann constant, Metrologia, [online],*https://tsapps.nist.gov/publication/getpdf.cfm?pubid* = 90764

[3] H. Felgner, O. Müller, and M. Schliwa, "Calibration of light forces in optical tweezers," Appl. Opt. 34(6), 977–982 (1995).

[4] J. L. Staff, Optical Trapping guide (2018), jLab E-Library, URL http://web.mit.edu/8.13/www/JLExperiments/JLExp51.pdf

[5] M. Haghshenas-Jaryani et al., "Dynamics of microscopic objects in optical tweezers: experimental determination of underdamped regime and numerical simulation using multiscale analysis," Nonlinear Dyn. 76(2), 1013–1030 (2014).

[6] P. Welch, "The use of fast Fourier transform for the estimation of power spectra: A method based on time averaging over short, modified periodograms," in IEEE Transactions on Audio and Electroacoustics, vol. 15, no. 2, pp. 70-73, June 1967, doi: 10.1109/TAU.1967.1161901.